Molecular Dynamics Simulations of Polyelectrolyte Brushes: From Single Chains to Bundles of Chains

ARTICLE *in* LANGMUIR · JANUARY 2008

Impact Factor: 4.46 · DOI: 10.1021/la702203c · Source: PubMed

3 AUTHORS:

Daniel J Sandberg
University of Connecticut
10 PUBLICATIONS **115** CITATIONS
SEE PROFILE

Jan-Michael Carrillo
Oak Ridge National Laboratory
63 PUBLICATIONS **576** CITATIONS
SEE PROFILE

Andrey V Dobrynin
University of Akron
124 PUBLICATIONS **4,903** CITATIONS
SEE PROFILE

Molecular Dynamics Simulations of Polyelectrolyte Brushes: From Single Chains to Bundles of Chains

Daniel J. Sandberg, Jan-Michael Y. Carrillo, and Andrey V. Dobrynin*

Polymer Program, Institute of Materials Science, Departments of Physics and Chemistry, University of Connecticut, Storrs, Connecticut 06269

Received July 20, 2007. In Final Form: September 4, 2007

Using molecular dynamics simulations in combination with scaling analysis, we have studied the effects of the solvent quality and the strength of the electrostatic interactions on the conformations of spherical polyelectrolyte brushes in salt-free solutions. The spherical polyelectrolyte brush could be in one of four conformations: (1) a star-like conformation, (2) a "star of bundles" conformation in which the polyelectrolyte chains self-assemble into pinned cylindrical micelles, (3) a micelle-like conformation with a dense core and charged corona, or (4) a conformation in which there is a thin polymeric layer uniformly covering the particle surface. These different brush conformations appear as a result of the fine interplay between electrostatic and monomer−monomer interactions. The brush thickness depends nonmonotonically on the value of the Bjerrum length. This dependence of the brush thickness is due to counterion condensation inside the brush volume. We have also established that bundle formation in poor solvent conditions for the polymer backbone can also occur in a planar polyelectrolyte brush. In this case, the grafted polyelectrolyte chains form hemispherical aggregates at low polymer grafting densities, cylindrical aggregates at an intermediate range of the grafting densities, and vertically oriented ribbon-like aggregates at high grafting densities.

1. Introduction

Polyelectrolyte brushes consist of charged polymers end-grafted to substrates of different geometries.[1−12] The grafted polyelectrolyte layers have found applications in colloidal stabilization, drug delivery, biocompatible coatings, pH-controlled gate devices (filters), "smart surfaces" (with responses determined by the surrounding environment), and biosensor technology (for review, see refs 1, 5, 7, and 8). These applications utilize the ability to control the brush morphology by changing the solvent quality for the polymer backbone, the polymer grafting density, the solutions' pH and salt concentration, and the dielectric properties of the solvent.

The experimental,[2,4−7,9,12−15] theoretical,[1,10,11,16−27] and computational[18,28−32] studies of polyelectrolyte brushes have established how the thickness of the polymeric layer and internal brush structure depends on the system parameters such as polymer grafting density, fraction of charged monomers on the polymer backbone, polymer−solvent affinity, and pH and ionic strength of the solutions. At low salt concentrations, for most experimentally relevant chain grafting densities, the counterions condensed inside the brush determine the thickness of the brush layer. In this regime, the deformation of the grafted polyelectrolyte chains is caused by the osmotic pressure localized within the brush counterions. This counterion osmotic force is balanced by the chain's elastic energy. The unique feature of this so-called "osmotic brush" regime is that the thickness of the brush shows only a weak dependence on the brush grafting density.[1,7,8] The direct measurements of the osmotic pressure of dilute solutions of the spherical polyelectrolyte brushes have shown that 95% of counterions are condensed inside the brush, resulting in a strong elongation of the grafted polyelectrolyte chains.[33,34] Addition of salt leads to screening of the electrostatic interactions inside the brush such that, at sufficiently high salt concentrations, the properties of the polyelectrolyte brush become similar to those of the neutral polymeric brush with the effective monomer−monomer second virial coefficient determined by the local salt concentration. In this high salt concentration regime, the thickness

(1) Balazs, A. C. et al. *Prog. Surf. Sci.* **1997**, *55*, 181−269.
(2) Azzaroni, O.; Moya, S.; Farhan, T.; Brown, A. A.; Huck, W. T. S. *Macromolecules* **2005**, *38*, 10192−10199.
(3) Bright, J. N.; Woolf, T. B.; Hoh, J. H. *Prog. Biophys. Mol. Biol.* **2001**, *76*, 131−173.
(4) Gelbert, M.; Biesalski, M.; Ruhe, J.; Johannsmann, D. *Langmuir* **2000**, *16*, 5774−5784.
(5) Minko, S. *Polym. Rev.* **2006**, *46*, 397−420.
(6) Raviv, U. et al. *Nature* **2003**, *425*, 163−165.
(7) Ruhe, J. et al. *Adv. Polym. Sci.* **2004**, *165*, 79−150.
(8) Ballauff, M.; Borisov, O. V. *Curr. Opin. Colloid Inteface Sci.* **2006**, *11*, 316−323.
(9) Romet-Lemonne, G.; Daillant, J.; Guenoun, P.; Yang, J.; Mays, J. W. *Phys. Rev. Lett.* **2004**, *93*, 148301-1-4.
(10) Borisov, O. V.; Birshtein, T. M.; Zhulina, E. *J. Phys. II* **1991**, *1*, 521−526.
(11) Pincus, P. *Macromolecules* **1991**, *24*, 2912−2919.
(12) Ahrens, H.; Förster, S.; Helm, C. A.; Kumar, N. A.; Naji, A.; Netz, R. R.; Seidel, C. *J. Phys. Chem. B* **2004**, *108*, 16870−16876.
(13) Farhan, T.; Azzaroni, O.; Huck, W. T. S. *Soft Matter* **2005**, *1*, 66−68.
(14) Hu, T. J.; You, Y. Z.; Pan, C. Y.; Wu, C. *J. Phys. Chem. B* **2002**, *106*, 6659−6662.
(15) Tran, Y.; Auroy, P.; Lee, L. T. *Macromolecules* **1999**, *32*, 8952−8964.
(16) Harden, J. L. *Macromolecules* **1997**, *30*, 5930−5938.
(17) Misra, S.; Tirrell, M.; Mattice, W. *Macromolecules* **1996**, *29*, 6056−6060.
(18) Naji, A.; Seidel, C.; Netz, R. R. In *Surface-Initiated Polymerization*; Jordan, R., Ed.; Advances in Polymer Science Series 198; Springer: New York, 2006; pp 149−183.
(19) Netz, R. R.; Andelman, D. *Phys. Rep.* **2003**, *380*, 1−95.
(20) Pickett, G. T.; Balazs, A. C. *Langmuir* **2001**, *17*, 5111−5117.
(21) Pryamitsyn, V. A.; Leermakers, F. A. M.; Fleer, G. J.; Zhulina, E. B. *Macromolecules* **1996**, *29*, 8260−8270.
(22) Csajka, F. S.; Seidel, C. *Macromolecules* **2005**, *38*, 2022.
(23) von Goeler, F.; Muthukumar, M. *J. Chem. Phys.* **1996**, *105*, 11335−11346.
(24) Zhulina, E.; Singh, C.; Balazs, A. C. *J. Chem. Phys.* **1998**, *108*, 1175−1183.
(25) Zhulina, E. B.; Borisov, O. V. *Macromolecules* **1996**, *29*, 2618−2626.
(26) Zhulina, E. B.; Borisov, O. V.; Birshtein, T. M. *Macromolecules* **1999**, *32*, 8189−8196.
(27) Zhulina, E. B.; Borisov, O. V. *J. Chem. Phys.* **1997**, *107*, 5952−5967.
(28) Kumar, N. A.; Seidel, C. *Macromolecules* **2005**, *38*, 9341−9350.
(29) Naji, A.; Netz, R. R.; Seidel, C. *Eur. Phys. J. E* **2003**, *12*, 223−237.
(30) Seidel, C. *Macromolecules* **2003**, *36*, 2536−2543.
(31) Crozier, P. S.; Stevens, M. J. *J. Chem. Phys.* **2003**, *118*, 3855−3860.
(32) Csajka, F. S.; Seidel, C. *Macromolecules* **2000**, *33*, 2728−2739.
(33) Wittemann, A.; Drechsler, M.; Talmon, Y.; Ballauff, M. *J. Am. Chem. Soc.* **2005**, *127*, 9688−9689.
(34) Das, B.; Guo, X.; Ballauff, M. *Prog. Colloid Polym. Sci.* **2002**, *121*, 34−38.

10.1021/la702203c CCC: $37.00
Published on Web 10/31/2007 PAGE EST: 12.9

of the planar polyelectrolyte brush decreases with increasing salt concentration as $c_s^{-1/3}$.[8,35] The solvent quality for the polymer backbone is one of the most important parameters controlling the brush morphology.[1] For example, in poor solvent conditions for the polymer backbone, polyelectrolyte chains forming a brush could be in the necklace-like conformation, form a dense polymeric layer, or self-assemble into pinned spherical micelles.[1,20,24] These different brush morphologies optimize the electrostatic interactions between ionized groups, counterion configurational entropy, and solvophobic interactions between the polymer and surrounding solvent. In response to these morphological transformations, the brush thickness demonstrates an abrupt change, indicating that the transition between different brush morphologies is a first-order transition. The collapse of the polyelectrolyte brush can also be induced by adding multivalent ions.

Coarse-grained computer simulations of the planar polyelectrolyte brush were performed by Seidel et al.[28−30,32] In these simulations, counterions and salt ions were included explicitly. However, the solvent is treated implicitly by introducing the macroscopic value of the dielectric constant of the medium which determines the strength of the electrostatic interactions. The short-range Lennard−Jones interactions between any particles in such simulations represent effective interactions. These simulations have shown that in the case of the strongly charged polyelectrolyte brush the counterions are localized within the brush, resulting in strong elongation of the polyelectrolyte chains forming a brush layer. This regime is usually referred to as the "osmotic brush" regime. The brush thickness in the osmotic brush regime shows a weak dependence on the brush grafting density with the exponent 1/5. The thickness of the brush depends nonmonotonically on the strength of the electrostatic interactions. With an increasing strength of the electrostatic interactions, the thickness of the brush layer first increases, and then it begins to decrease as the strength of the electrostatic interactions increases further. This decrease in the brush thickness is due to counterion condensation on the polyelectrolyte chains. Note that experimentally the strength of the electrostatic interactions can also be changed by changing the dielectric constant of the medium. Addition of salt leads to screening of the electrostatic interactions between the brush molecules, which is manifested in the decrease of the brush thickness with salt concentration as $c_s^{-1/3}$. This salt concentration dependence of the brush thickness is in agreement with theoretical predictions for the osmotic brush regime. Unfortunately, the effect of the solvent quality for the polymer backbone and the strength of the electrostatic interactions on the morphology of the polyelectrolyte brush have not been studied in these simulations.

In this paper, we study the effect of the solvent quality for the polymer backbone and the strength of the electrostatic interactions on conformations of the polyelectrolyte brush grafted to a spherical particle (spherical brush). Using a combination of molecular dynamics simulations and scaling analysis, we have established the range of parameters for which a spherical polyelectrolyte brush can be in a star-like spherical conformation, have a "star of bundles" conformation in which polyelectrolyte chains self-assemble into clusters of pinned cylindrical micelles with the axis of the axial symmetry of the cylinder pointing along the normal to the surface of the spherical particle, have a micelle-like conformation with a dense core and charged corona, and form a thin polymeric layer uniformly covering the particle surface. All these different brush morphologies appear as a result of competition between counterion configurational entropy,

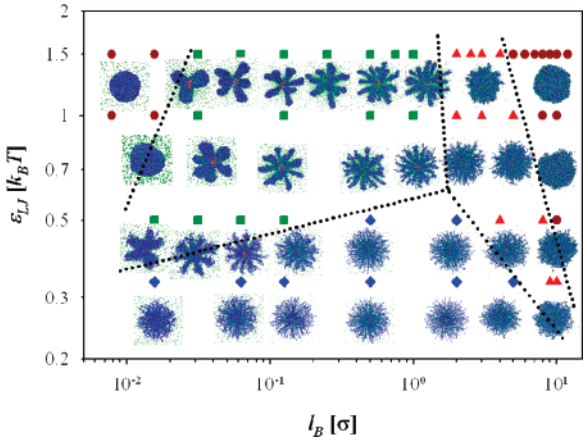

Figure 1. Diagram of states of spherical polyelectrolyte brushes with degree of polymerization $N = 60$ and a fraction of charged monomers $f = 1/3$: collapsed brushes (circles), bundle brushes (squares), star-like brushes (tilted squares), and micelle-like brushes (triangles). The dotted lines separating different conformational regimes are not actual phase transition lines.

solvent quality for the polymer backbone, and the strength of the electrostatic interactions. To show that the pinned cylindrical micelles are not specific to the spherical structure of the grafted layer, we have performed molecular dynamics simulations of the planar brush at the same grafting densities. In these simulations, we have also observed self-assembly of the polyelectrolyte chains into pinned cylindrical micelles. The rest of the manuscript is organized as follows. In section 2, we present the results of the molecular dynamics simulations of the spherical polyelectrolyte brush in salt-free solution and compare them with the predictions of the scaling model of the spherical brush. At the end of the section, we briefly discuss the planar brush behavior. Finally, in section 3, we summarize our results.

2. Molecular Dynamics Simulations of Polyelectrolyte Spherical and Planar Brushes

2.1. Simulation Details. We performed molecular dynamics simulations of spherical polyelectrolyte brushes with explicit counterions. The flexible polyelectrolytes were modeled by chains of charged Lennard−Jones (LJ) particles (beads) with diameter σ, degree of polymerization $N = 60$, and fraction of the charged monomers $f = 1/3$ corresponding to every third monomer carrying a negative electrical charge, $-e$. Polyelectrolyte chains, $M = 184$, were attached by one end to the spherical particle with radius 5.14σ at a grafting density $0.555\sigma^{-2}$. The surface of the spherical particle was formed by $N_p = 367$ overlapping beads with diameter σ. To neutralize $M = 184$ negatively charged polyelectrolyte chains, 3680 positively charged counterions were added in the simulation box.

All particles in the system interacted through the truncated-shifted Lennard−Jones (LJ) potential:

$$U_{LJ}(r_{ij}) = \begin{cases} 4\epsilon_{LJ}\left[\left(\frac{\sigma}{r_{ij}}\right)^{12} - \left(\frac{\sigma}{r_{ij}}\right)^{6} - \left(\frac{\sigma}{r_{cut}}\right)^{12} + \left(\frac{\sigma}{r_{cut}}\right)^{6}\right] & r \le r_{cut} \\ 0 & r > r_{cut} \end{cases} \quad (1)$$

where r_{ij} is the distance between the ith and jth beads and σ is the bead diameter chosen to be the same regardless of the bead type. The cutoff distance, $r_{cut} = 2.5\sigma$, was chosen for polymer−polymer interactions, and $r_{cut} = \sqrt[6]{2}\sigma$ was chosen for all other pairwise interactions. The interaction parameter ϵ_{LJ} was equal

(35) Ahrens, H.; Förster, S.; Helm, C. A. *Phys. Rev. Lett.* **1998**, *81*, 4172−4175.

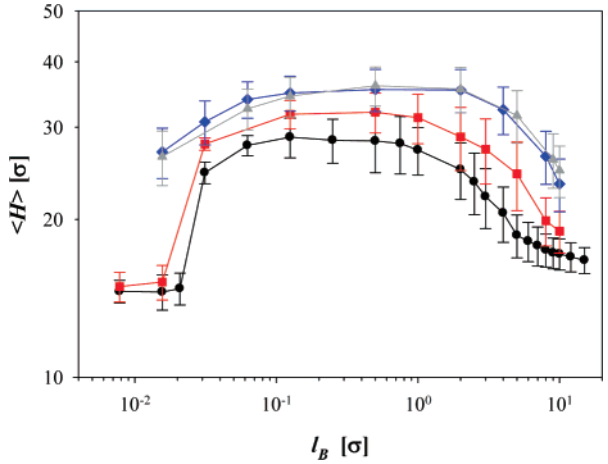

Figure 2. Dependence of the brush thickness on the value of the Bjerrum length for weakly charged, $f = 1/3$, spherical brushes at different values of the Lennard−Jones interaction parameter: $\epsilon_{LJ} = 1.5k_BT$ (circles), $\epsilon_{LJ} = 1.0k_BT$ (squares), $\epsilon_{LJ} = 0.5k_BT$ (tilted squares), and $\epsilon_{LJ} = 0.333k_BT$ (triangles).

to k_BT for polymer−particle, polymer−counterion, counterion−counterion, and counterion−particle interactions, where k_B is the Boltzmann constant and T is the absolute temperature. The value of the Lennard−Jones interaction parameter for the polymer−polymer pair was varied between $0.33k_BT$ and $1.5k_BT$, which allowed a change in the solvent quality for the polymer backbone between theta and poor solvent conditions.

The connectivity of beads in polyelectrolyte chains was maintained by the finite extension nonlinear elastic (FENE) potential:

$$U_{FENE}(r) = -\frac{1}{2}k_{spring}R_{max}^{\ 2}\ln\left(1 - \frac{r^2}{R_{max}^{\ 2}}\right) \qquad (2)$$

with the spring constant $k_{spring} = 30k_BT/\sigma^2$, where $R_{max} = 1.5\sigma$ is the maximum bond length. The combination of FENE and LJ potentials prevents the bonds from crossing each other during the simulation run.

Interaction between any two charged beads with charge valences q_i and q_j, and separated by a distance r_{ij}, is given by the Coulomb potential

$$U_{Coul}(r_{ij}) = k_BT\frac{l_Bq_iq_j}{r_{ij}} \qquad (3)$$

where $l_B = e^2/\epsilon k_BT$ is the Bjerrum length, defined as the length scale at which the Coulomb interaction between two elementary charges e, in a dielectric medium with the dielectric constant ϵ, is equal to the thermal energy k_BT. In our simulations, the value of the Bjerrum length l_B was varied between 1/64 and 15σ.

The particle-particle particle-mesh (PPPM) method[36] implemented in LAMMPS,[37] with the sixth-order charge interpolation scheme and estimated accuracy 10^{-5}, was used for calculations of the electrostatic interactions between all charges in the system.

Simulations were carried out in a constant number of particles, volume, and temperature (NVT) ensemble with periodic boundary conditions.[36] The spherical brush was fixed in the center of the cubic simulation box with size $L = 140\sigma$. The constant

(36) Frenkel, D.; Smit, B. *Understanding molecular simulations*; Academic Press: San Diego, 2001.
(37) Plimpton, S. *LAMMPS User's Manual*; Sandia National Laboratory: Albuquerque, NM, 2005.

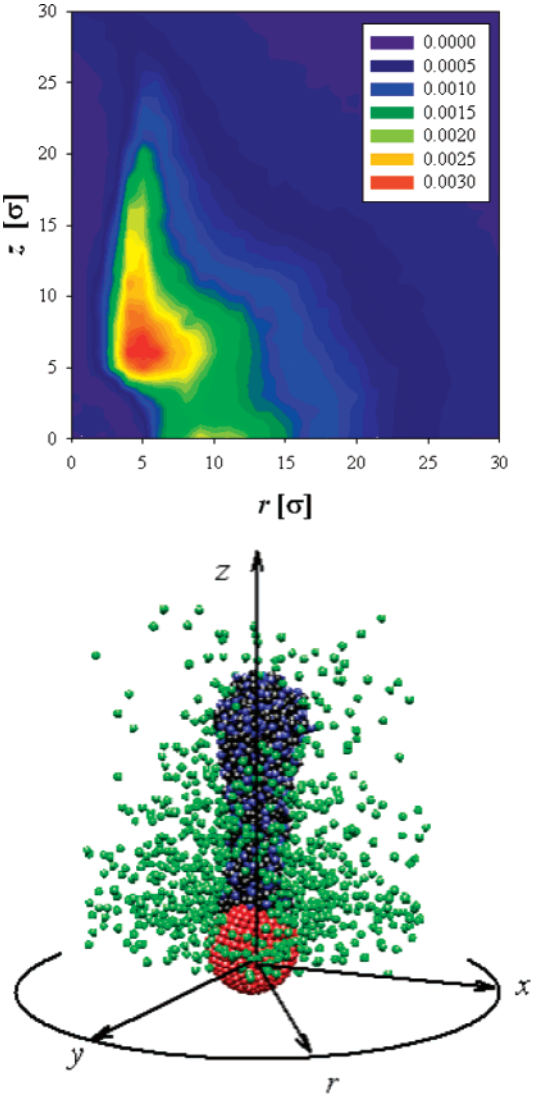

Figure 3. Spatial distribution of the counterion density $\rho(z,r)\sigma^3$ around a bundle of polyelectrolyte chains for $\epsilon_{LJ} = 1.5k_BT$ and $l_B = 0.125\sigma$. The snapshot shows the distribution of counterions around a bundle.

temperature was maintained by coupling the system to a Langevin thermostat.[36] In this case, the equation of motion of the ith particle is

$$m\frac{d\vec{v}_i(t)}{dt} = \vec{F}_i(t) - \xi\vec{v}_i(t) + \vec{F}_i^{\,R}(t) \qquad (4)$$

where $\vec{v}_i$ is the bead velocity and $\vec{F}_i$ is the net deterministic force acting on the ith bead of mass m. $\vec{F}_i^{\,R}$ is the stochastic force with zero average value $\langle\vec{F}_i^{\,R}(t)\rangle = 0$ and δ-functional correlations $\langle\vec{F}_i^{\,R}(t)\,\vec{F}_i^{\,R}(t')\rangle = 6\xi k_BT\delta(t - t')$. The friction coefficient ξ was set to $\xi = m/\tau_{LJ}$, where τ_{LJ} is the standard LJ-time $\tau_{LJ} = \sigma(m/\epsilon_{LJ})^{1/2}$. The velocity−Verlet algorithm with a time step $\Delta t = 0.01\tau_{LJ}$ was used for integration of the equations of motion (eq 4).

Simulations were performed using the following procedure: At the beginning of each simulation run, a spherical particle with grafted polyelectrolyte chains was fixed at the center of the simulation box. Polyelectrolyte chains were grafted to the particle in the fully extended conformation pointing in the radial direction from the center of the particle. Neutralizing monovalent counterions were uniformly distributed over the volume of the

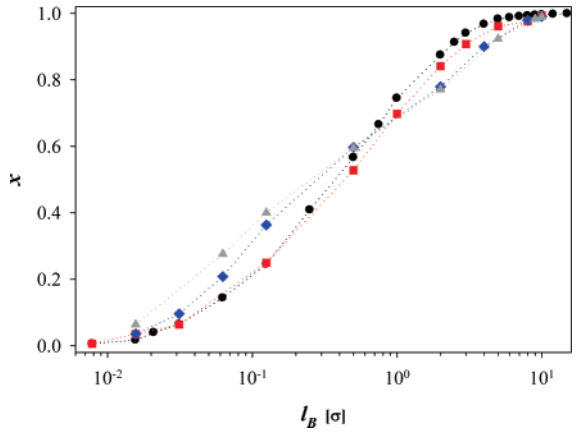

Figure 4. Dependence of the fraction of the condensed counterions x on the value of the Bjerrum length for weakly charged, $f = 1/3$, spherical brushes at different values of the Lennard−Jones interaction parameter: $\epsilon_{LJ} = 1.5k_BT$ (circles), $\epsilon_{LJ} = 1.0k_BT$ (squares), $\epsilon_{LJ} = 0.5k_BT$ (tilted squares), and $\epsilon_{LJ} = 0.333k_BT$ (triangles).

simulation box. The system was pre-equilibrated for 10^6 molecular dynamics (MD) steps. This was followed by the production run lasting 3×10^6 MD steps. During the production run, we averaged the brush thickness and the fraction of condensed counterions, determined the counterion distribution function, and determined the distribution function of the number of chains forming bundles (bundle aggregation number).

In addition to simulations of the spherical brush, molecular dynamics simulations of the planar brush with grafting densities between $0.012\sigma^{-2}$ and $0.231\sigma^{-2}$ were performed. The grafting surface was modeled by a periodic hexagonal packed lattice of beads with diameter σ located at $z = 0$. A similar nonselective surface was located at the opposite side of the simulation box to prevent counterions from escaping and, hence, maintaining 2D periodicity in the lateral (x and y) directions. The system size in the xy-plane was equal to $84.0\sigma \times 86.6\sigma$. The height of the simulation box was 85.3σ. The interaction parameters for these simulations were identical to those used for spherical brush simulations.

The particle-particle particle-mesh (PPPM) method for the slab geometry implemented in LAMMPS[37] with the sixth-order charge interpolation scheme was used to calculate the electrostatic interactions in the system. In this method, the 2D periodic images of the system are periodically replicated along the z-direction with a distance $L = 3L_z$ between their boundaries. This reduces the problem of calculation of the electrostatic interactions in a 2D periodic system to those in a 3D system.

The simulation protocol was similar to the one described above for the spherical brush simulations.

2.2. Simulation Results. Figure 1 summarizes different conformational regimes of the spherical brush as a function of the solvent quality for the polymer backbone, which is controlled by the value of the Lennard−Jones interaction parameter ϵ_{LJ}, for the simulations without an explicit solvent and the value of the Bjerrum length, l_B. The charged spherical brush can be in four different conformational regimes: star-like brush, star formed by the bundles of the polyelectrolyte chains, micelle-like brush, and collapsed brush. The transitions between these conformational regimes are controlled by both the strength of the electrostatic interactions and the value of the Lennard−Jones interaction parameter. For small values of the Bjerrum length and large values of the Lennard−Jones interaction parameter, $\epsilon_{LJ} > 0.5$, a polyelectrolyte brush collapses, forming a dense polymeric layer covering the central nanoparticles. The chain's collapse is

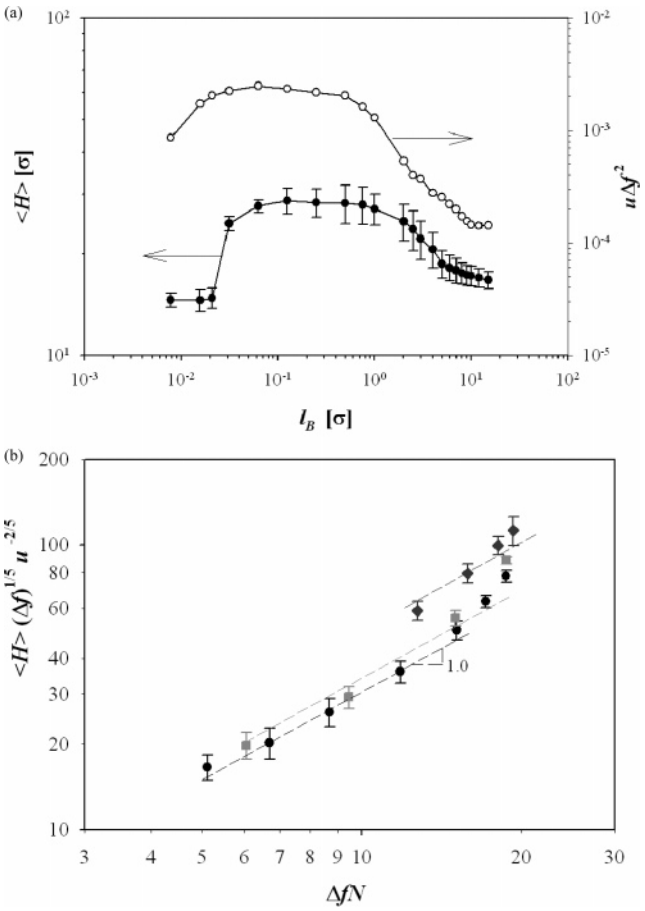

Figure 5. (a) Dependence of the interaction parameter $u\Delta f^2$ (open symbols) and brush thickness (filled symbols) on the value of the Bjerrum length for $\epsilon_{LJ} = 1.5k_BT$. (b) Dependence of the reduced brush thickness on the effective chain valence ΔfN for spherical polyelectrolyte brushes at different values of the Lennard−Jones interaction parameters: $\epsilon_{LJ} = 1.5k_BT$ (circles), $\epsilon_{LJ} = 1.0k_BT$ (squares), and $\epsilon_{LJ} = 0.5k_BT$ (tilted squares).

due to short-range monomer−monomer attractions that are stronger than the electrostatic repulsion between charged monomers. By collapsing, the chains forming a brush maximize the number of favorable monomer−monomer contacts. As the value of the Bjerrum length, l_B, increases, the strength of the electrostatic interactions between charged monomers increases as well. This increase of the electrostatic interactions first leads to deformation of the shape of the collapse brush, resulting in its elongation. The shape deformation minimizes the electrostatic repulsion but at the same time maximizes the surface energy contribution to the brush free energy in comparison with that for the spherical collapsed brush. The spherical collapsed brush becomes unstable when the value of the Bjerrum length exceeds a critical value $(l_B)_{CB} \approx \sigma(|\tau|/f^2 N_{ch} N)$. Note that at the transition value of the Bjerrum length the surface energy of the collapsed polyelectrolyte brush becomes on the order of the brush electrostatic energy (for details, see Appendix A). It is interesting to point out that the problem of stability of the collapsed polyelectrolyte brush is similar to the problem of the stability of the charged liquid droplet and a collapsed polyelectrolyte chain in poor solvent.[38−45] The transition from the collapsed

(38) Dobrynin, A. V.; Rubinstein, M.; Obukhov, S. P. *Macromolecules* **1996**, *29*, 2974−2979.
(39) Dobrynin, A. V.; Rubinstein, M. *Macromolecules* **1999**, *32*, 915−922.
(40) Lyulin, A. V.; Dunweg, B.; Borisov, O. V.; Darinskii, A. A. *Macromolecules* **1999**, *32*, 3264−3278.
(41) Limbach, H. J.; Holm, C. *J. Phys. Chem. B* **2003**, *107*, 8041−8055.

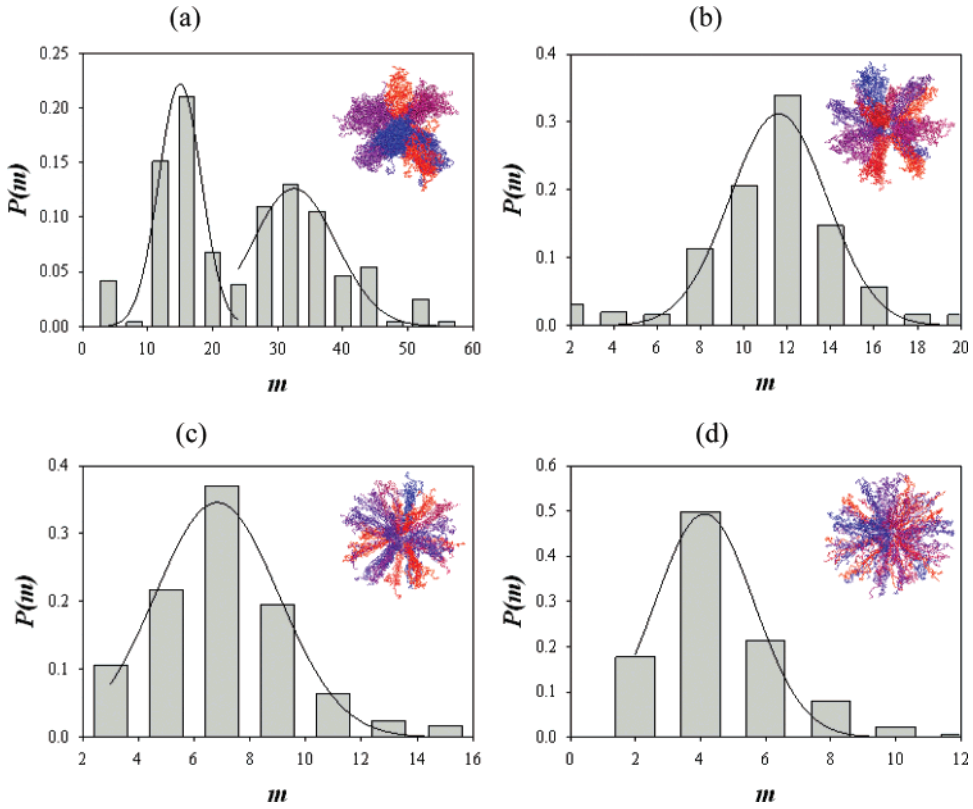

Figure 6. Distribution function of the bundle aggregation number m for weakly charged, $f = 1/3$, spherical brushes at the value of Lennard−Jones interaction parameter $\epsilon_{LJ} = 0.5k_BT$ and at different values of the Bjerrum length $l_B = 0.0156\sigma$ (a), $l_B = 0.0312\sigma$ (b), $l_B = 0.0625\sigma$ (c), and $l_B = 0.125\sigma$ (d). Insets show the typical star of bundles conformation.

state is clearly seen in the dependence of the brush thickness on the Bjerrum length (see Figure 2), which shows an abrupt increase when the value of the Bjerrum length exceeds $l_B = 1/32\sigma$ for $\epsilon_{LJ} = 1.5k_BT$. Note that the sharpness of the transition decreases with a decreasing value of the Lennard−Jones interaction parameter. For smaller values of the parameter ϵ_{LJ}, the polyelectrolyte chains are less collapsed, which results in a thicker polymeric layer covering the central spherical particle.

For larger values of the Bjerrum length, the polyelectrolyte brush in the poor solvent conditions for the polymer backbone adopts a star of bundles conformation (see Figure 1). The placement of the charges into the arms of the star achieves the maximum possible separation between charged monomers and lowers the electrostatic repulsion between them. However, such chain placement creates additional interfacial area separating the dense polymeric regions from the polymer free space. This results in an increase of the system surface energy. The formation of the star of bundles conformation is a result of the optimization of the electrostatic and surface energies of grafted polyelectrolyte chains (see Appendix A).

The brush thickness in this regime first increases with an increasing value of the Bjerrum length and then remains approximately constant (see Figure 2). This peculiar behavior of the brush thickness is a result of counterion condensation.[46,47] The counterions are distributed nonuniformly over the brush volume, which can be clearly seen in Figure 3. The counterions are predominantly accumulated close to the surface of the central nanoparticles. This correlates well with the concentration of the charged monomers, which is largest close to the surface of the spherical nanoparticles. The higher concentration of the charged monomers corresponds to the lowest value of the electrostatic potential driving the counterion condensation. It is interesting to point out that these condensed counterions play the role of the nucleating agents that facilitate the formation of the dense polymeric core surrounding the central nanoparticles in the micellar regime when a polyelectrolyte brush adopts a micelle-like conformation (see discussion below).

The dependence of the fraction of the condensed counterions on the value of the Bjerrum length is shown in Figure 4. To obtain the fraction of the condensed counterions for this plot, we have surrounded each monomer by a sphere of radius $r_c = 2.5\sigma$ and counted all counterions with a center of mass within this cutoff distance from a monomer. The final list of the condensed counterions was examined for multiple entries such that each condensed counterion was counted only once. The fraction of condensed counterions increases with increasing Bjerrum length for all values of the Lennard−Jones interaction parameter ϵ_{LJ}. At small values of the Bjerrum length, $l_B < 0.04\sigma$, more than 80% of the counterions leave the brush. In this interval of the Bjerrum length, the counterion configurational entropy loss due to localization within a brush is much larger than the electrostatic attraction of a counterion to a polyelectrolyte chain. The fraction of the condensed counterions increases to about 50% at a value of the Bjerrum length $l_B \approx 0.8\sigma$. At this value of the Bjerrum length, the configurational entropy loss is on the order of the electrostatic energy gain due to counterion condensation. For the value of the Bjerrum length, $l_B = 8\sigma$, about 95% of counterions are condensed on the polymer backbone. For this value of the

(42) Liao, Q.; Dobrynin, A. V.; Rubinstein, M. *Macromolecules* **2006**, *39*, 1920−1938.
(43) Jeon, J.; Dobrynin, A. V. *J. Phys. Chem. B* **2006**, *110*, 24652−24665.
(44) Dobrynin, A. V.; Rubinstein, M. *Prog. Polym. Sci.* **2005**, *30*, 1049−1118.
(45) Micka, U.; Kremer, K. *Europhys. Lett.* **2000**, *49*, 189−195.
(46) Oosawa, F. *Polyelectrolytes*; Marcel Dekker: New York, 1971.
(47) Manning, G. S. *J. Chem. Phys.* **1969**, *51*, 924−933.

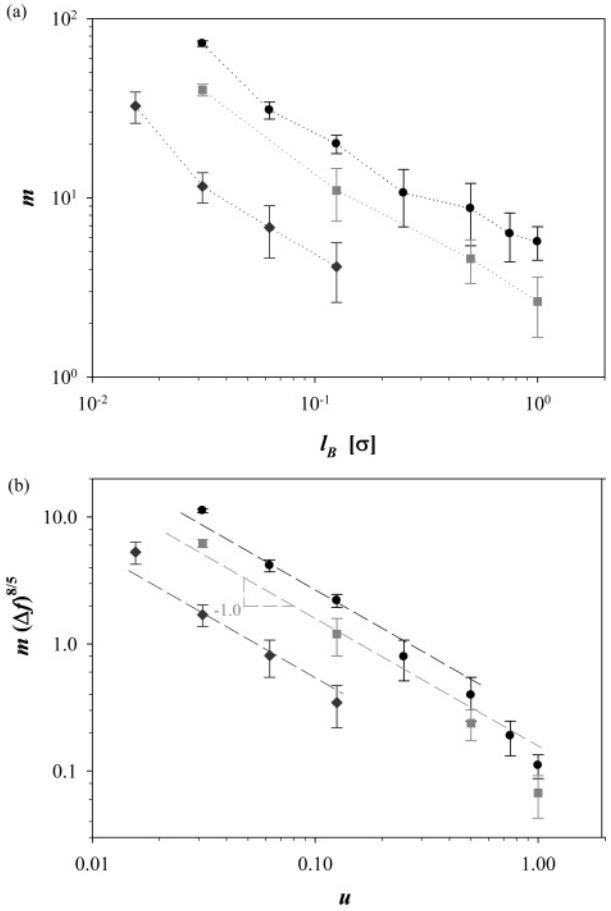

Figure 7. (a) Dependence of the bundle aggregation number m on the value of the Bjerrum length for weakly charged, $f = 1/3$, spherical brushes at different values of the Lennard−Jones interaction parameter: $\epsilon_{LJ} = 1.5k_BT$ (circles), $\epsilon_{LJ} = 1.0k_BT$ (squares), and $\epsilon_{LJ} = 0.5k_BT$ (tilted squares). (b) Dependence of the reduced aggregation number $m\Delta f^{8/5}$ on the parameter u. Notations are the same as those in part (a).

Bjerrum length, the electrostatic contribution to the counterion free energy is much larger than its configurational entropy part.

Figure 4 shows a significant effect of the solvent quality for the polymer backbone on the fraction of the condensed counterions. Note that, at small values of the Bjerrum length, $l_B < 1\sigma$, the fraction of the condensed counterions increases monotonically with decreasing value of the Lennard−Jones interaction parameter ϵ_{LJ}. With an increasing value of the Lennard−Jones interaction parameter, the local polymer density increases. Thus, placing counterions inside the brush will create more unfavorable counterion−monomer contacts in the dense brush compared to the brush with a lower monomer concentration. It is also important to point out that in the case of the star of bundles configuration most of the condensed counterions are distributed outside the dense polymeric domains (see Figure 3). The situation qualitatively changes for $l_B > 1\sigma$. In this interval of the Bjerrum length, the electrostatic interactions between the charged monomer and condensed counterions are stronger than the short-range monomer−counterion interactions. In the dense polyelectrolyte brush, the local charge concentration is higher than that in the polyelectrolyte brush with a lower polymer concentration, which corresponds to a lower value of the local electrostatic potential and promotes additional counterion condensation inside the brush. In this interval of the Bjerrum length, the fraction of condensed counterions is highest for the system with the largest value of the Lennard−Jones interactions parameter, $\epsilon_{LJ} = 1.5k_BT$.

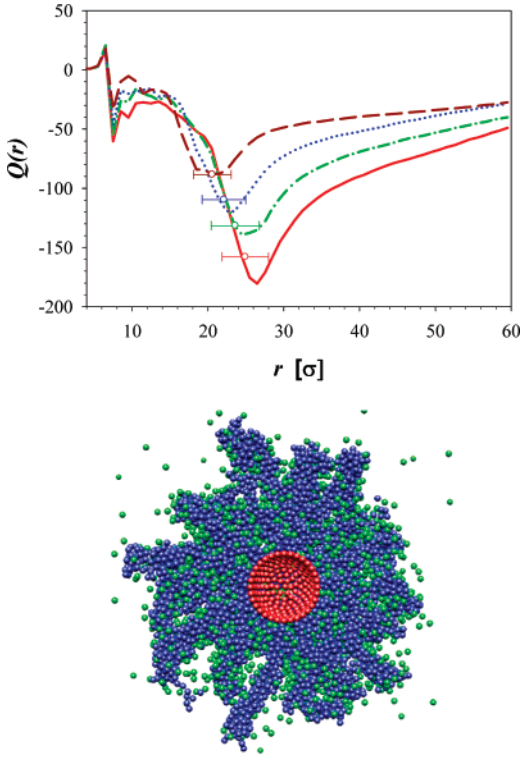

Figure 8. Radial distribution of the accumulated charge of the micelle-like brush structure for the value of the Lennard−Jones interaction parameter $\epsilon_{LJ} = 1.5k_BT$ and different values of the Bjerrum lengths: $l_B = 2.0\sigma$ (red solid line), $l_B = 2.5\sigma$ (green dash-dotted line), $l_B = 3.0\sigma$ (blue dotted line), $l_B = 4.0\sigma$ (brown dashed line), and the locations of the corresponding brush thicknesses are shown by circles. The inset shows the cross section of the snapshot of the micelle-like brush structure at the value of the Bjerrum length $l_B = 3.0\sigma$. The beads forming the central nanoparticle are shown in red, the polymer chains are colored in blue, and the counterions are shown in green.

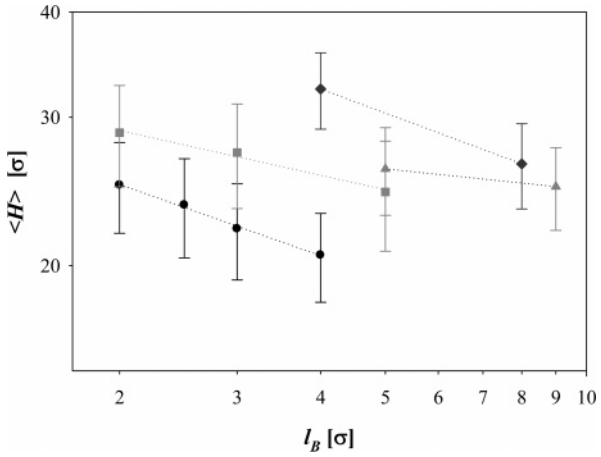

Figure 9. Dependence of the thickness of the micelle-like brush at different values of the Lennard−Jones interaction parameter: $\epsilon_{LJ} = 1.5k_BT$ (circles), $\epsilon_{LJ} = 1.0k_BT$ (squares), $\epsilon_{LJ} = 0.5k_BT$ (tilted squares), and $\epsilon_{LJ} = 0.333k_BT$ (triangles). The brush thickness shows a power law dependence on the value of the Bjerrum length with exponents −0.28 and −0.18 for $\epsilon_{LJ} = 1.5k_BT$ and $\epsilon_{LJ} = 1.0k_BT$, respectively.

The scaling analysis of the brush thickness presented in Appendix A (see eq A20) shows that the fraction of the condensed counterions influences the brush structure through the value of the electrostatic interaction parameter $u\Delta f^2$, where u is the ratio of the Bjerrum length to bond size, $u = l_B/\sigma$ and $\Delta f = f(1 - x)$.

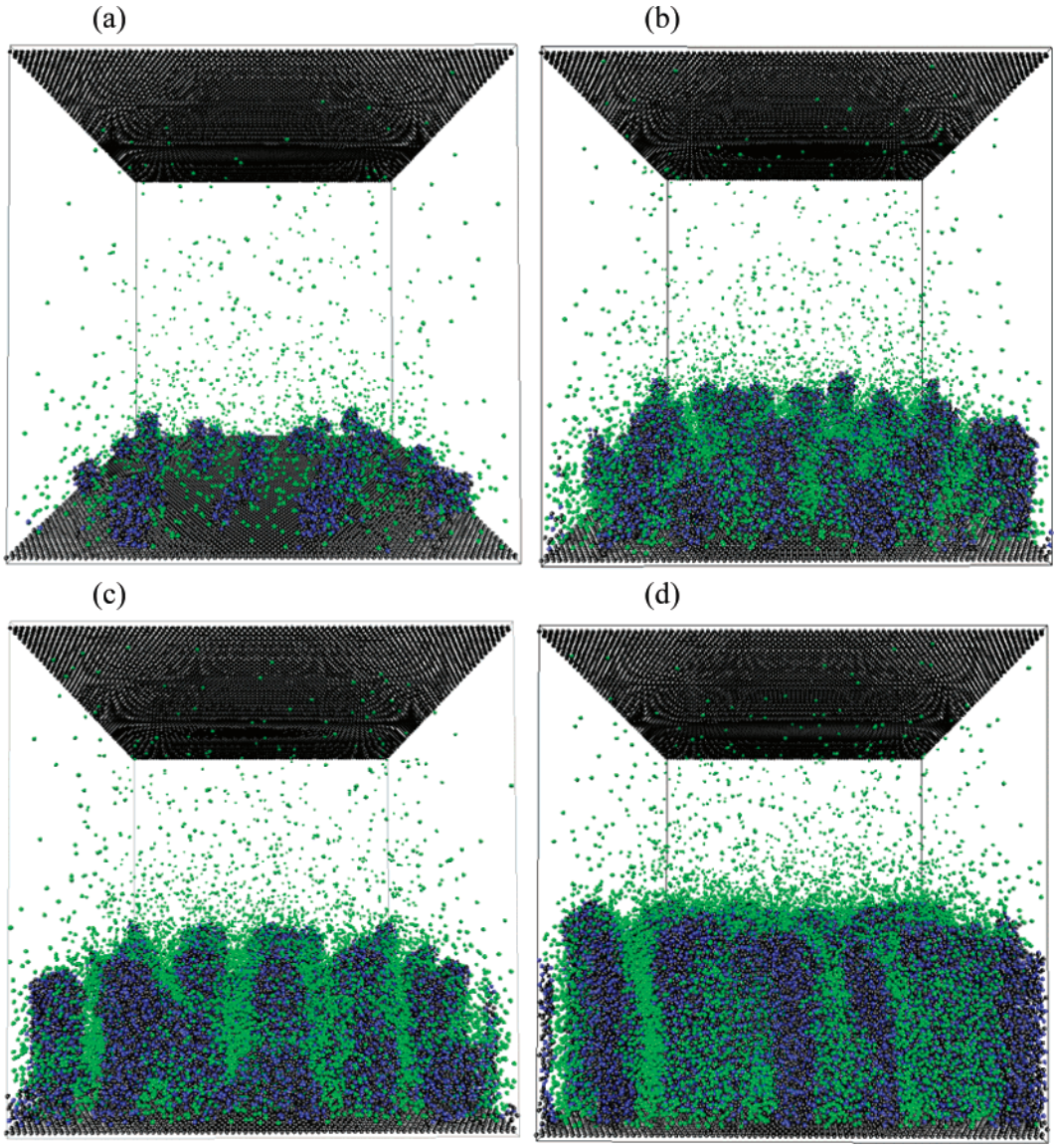

Figure 10. Typical conformations of the planar polyelectrolyte brush in poor solvent conditions for the polymer backbone, $\epsilon_{LJ} = 1.5k_BT$, at the value of the Bjerrum length $l_B = 0.125\sigma$, and at different grafting densities $\rho_g = 0.012\sigma^{-2}$ (a), $\rho_g = 0.058\sigma^{-2}$ (b), $\rho_g = 0.115\sigma^{-2}$ (c), and $\rho_g = 0.231\sigma^{-2}$ (d).

This can be clearly seen in Figure 5a which shows correlation between the brush thickness and the strength of the interaction parameter $u\Delta f^2$. For small values of the Bjerrum length, $l_B/\sigma < 1/16$, when the fraction of the condensed counterions is much smaller than unity, $x \ll 1$, the value of the interaction parameter is proportional to the value of the Bjerrum length. However, as the counterion condensation increases, the increase of the value of the Bjerrum length is compensated by the decrease in the effective fraction of the ionized groups, Δf. Thus, the unchanged region of the brush thickness is a result of the compensation of the increase of the Bjerrum length by the decrease of the effective charge fraction of the polyelectrolyte brush, Δf. To test the prediction of the scaling model for the brush thickness, $H \propto \sigma(u\Delta f^2)^{2/5}N$, in Figure 5b, we plotted the dependence of the reduced brush thickness $H\Delta f^{1/5}/u^{2/5}$ on the effective valence of the polyelectrolyte chain ΔfN. The data set corresponding to the value of the Lennard−Jones interaction parameter $\epsilon_{LJ} = 0.5k_BT$ shows a linear dependence of the reduced brush thickness on the chain valence. However, the data points for $\epsilon_{LJ} = 1.5k_BT$ and $1.0k_BT$ data sets deviate from straight lines at large values of the effective chain valence, ΔfN. For these values of the parameter ΔfN, the star of bundles has a small number of arms. For such stars, the brush thickness is determined by the intrabundle electrostatic interactions (see eqs A15 and A16), which have slightly different scaling dependences on the parameters u and Δf.

The distribution functions of the aggregation number of polyelectrolyte chains forming bundles show a finite size effect (see Figure 6). For small values of the Bjerrum length when the number of bundles is less than ten, the distribution function is bimodal. The first peak in the distribution function corresponds to six bundles located on the equator of the star, each of which has approximately 18 chains. The second peak in the distribution function corresponds to two bundles located at two poles of the star consisting of approximately 32 chains. With an increasing value of the Bjerrum length, the distribution function becomes unimodal with a single maximum. The peak position gradually shifts with increasing value of the Bjerrum length toward a smaller number of chains in the most probable bundle. Figure 7a combines the dependence of the most probable bundle aggregation number on the value of the Bjerrum length, l_B. In the case of the bimodal distribution function, we choose the value of the aggregation

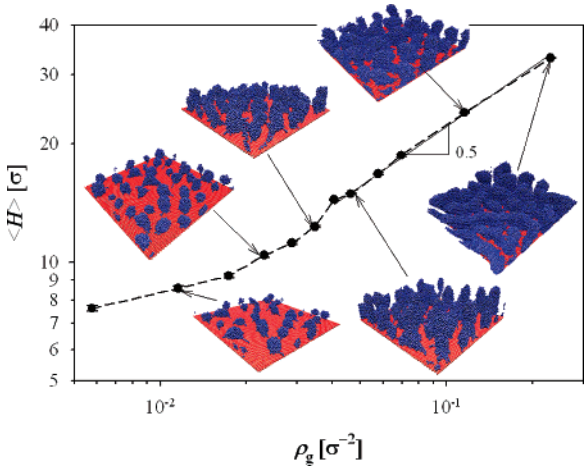

Figure 11. Dependence of the average brush thickness of the planar polyelectrolyte brush in poor solvent conditions for the polmer backbone, $\epsilon_{LJ} = 1.5k_BT$, and at the value of the Bjerrum length $l_B = 0.125\sigma$ on the brush grafting density. Insets show typical brush conformations.

number m corresponding to the peak with the largest amplitude. The bundle aggregation number also decreases with decreasing value of the Lennard−Jones interaction parameter. The decrease of the Lennard−Jones interaction parameter leads to a decrease of the surface energy of the polymer interface, thus decreasing the cost for creation of the additional surface area. The bundles disappear for the value of the Lennard−Jones interaction parameter $\epsilon_{LJ} = 0.33k_BT$, a value which is close to that of the θ-solvent conditions for the coarse-grained model used in our simulations.

The dependence of the bundle aggregation number on the interaction parameter $u\Delta f^2$ is given by eq A22, $m \propto (u\Delta f^2)^{-4/5}$. In Figure 7b, we have compared the results of the computer simulations with the predictions of the scaling model by plotting $m\Delta f^{8/5}$ against the parameter u. The simulation results show an inverse linear dependence of the parameter $m\Delta f^{8/5}$ on the value of the reduced Bjerrum length u. This dependence is stronger than the one expected from the scaling model which predicts $u^{-4/5}$ scaling. The difference in the scaling exponents can be attributed to the nonuniform counterion distribution within a brush which is neglected in the scaling model.

In the micelle-like conformation of the polyelectrolyte brush, the core of the micelle consists of both condensed counterions and sections of polyelectrolyte chains. The core of the micelle is almost neutral, while the excess polymeric charge is expelled into the corona. This can be clearly seen in Figure 8, which represents the dependence of the accumulated brush charge

$$Q(r) = 4\pi \int_R^r q(y) y^2 \, dy \qquad (5)$$

where $q(y)$ is the local number charge density. With an increasing value of the Bjerrum length, the core size increases by absorbing sections of the chains expelled into the corona. The small charge of the core is maintained by the condensation of more counterions. The core formation is driven by the strong correlation-induced attraction between condensed counterions and charged monomers. The origin of these attractive interactions is similar to those in strongly correlated Wigner liquids (for review, see refs 48 and 49) or in ionic crystals such as NaCl. For example, in the case of the ionic crystal, the attractive (negative) lattice energy is due to the spatial distribution (spatial correlations) of cations and anions over the lattice sites, even though the net charge of the crystal is zero. Note that the crystal will remain stable even if it carries a small nonzero charge because of the large lattice (correlation) energy. Finally, at very high values of the Bjerrum length (see Figure 1), all sections of the polyelectrolyte chains forming a brush condense and the thickness of the brush layer saturates. This collapsed polymeric layer is thicker than in the case of small l_B values because condensed counterions neutralize the polymer charge and fill a significant fraction of the layer volume. The formation of the micelle-like structure of the polyelectrolyte brush is a result of the fingering instability of the dense polymeric layer with counterions. This instability is qualitatively different from the Rayleigh type instability of charged objects.[44] The main feature of this instability is the expulsion of the excess charge into the corona of the micelle. Furthermore, this instability occurs at smaller charge asymmetries, $\Delta f_{FI} \propto f^{1/3}(N_{ch}N)^{-2/3}$, than the Rayleigh type instability, $\Delta f_{CB} \propto (N_{ch}N)^{-1/2}$, observed in the charged system for which the collapse is caused by short-range monomer−monomer attraction.[44]

The scaling dependence of the brush thickness in the micelle-like brush regime is shown in Figure 9. Unfortunately, for our chain length and grafting density, this regime is not wide enough to make definite conclusions about the validity of the scaling model. For the system with the value of the interaction parameter $\epsilon_{LJ} = k_BT$, the slope is close to the expected scaling value 0.2. However, for other values of the Lennard−Jones interaction parameter, the simulation data deviate from the scaling model predictions.

To the end of this section, let us point out that the bundle formation in poor solvent conditions for the polyelectrolyte brush backbone is not a specific feature of the spherical brush. These bundles can also be formed in cylindrical and planar polyelectrolyte brushes. Figure 10 shows the snapshots of the simulations of the planar polyelectrolyte brush in poor solvent conditions for the polymer backbone. At a small grafting density, the polyelectrolyte chains collapse, forming semispherical micelles. With an increasing chain grafting density, the electrostatic repulsion between neighboring chains increases, forcing micelles to elongate and to form cylindrical micelles with the axial symmetry axis directed normal to the grafting surface. One can think about this structure as a forest of cylindrical micelles. Note that the aggregation number of these micelles increases with increasing polymer grafting density. Eventually, the cylindrical micelles aggregate and form an interpenetrating system of the vertically standing ribbon-like aggregates spanning the whole system. The brush thickness first weakly increases with increasing brush grafting density, then it approaches a power law $H \propto \rho_g^{1/2}$ when the polyelectrolytes form cylindrical and ribbon-like aggregates (see Figure 11). The brush thickness for this plot was obtained from the first moment of the polymer density distribution $\rho(z)$

$$H = 2\int_0^{L_z} z\, \rho(z)\, dz / \int_0^{L_z} \rho(z)\, dz \qquad (6)$$

Note that, at low and intermediate brush grafting densities, the aggregation number and thickness of the cylindrical micelles is controlled by intramicellar electrostatic interactions. A more detailed study of the planar polyelectrolyte brush will be presented in a future publication.

3. Conclusions

The effect of the solvent quality and the strength of the electrostatic interactions on the conformational transformations

(48) Grosberg, A. Y.; Nguyen, T. T.; Shklovskii, B. I. *Rev. Mod. Phys.* **2002**, *74*, 329−345.
(49) Levin, Y. *Rep. Prog. Phys.* **2002**, *65*, 1577−1632.

in polyelectrolyte brushes have been studied. Using molecular dynamics simulations and scaling analysis, we have established that the polyelectrolyte spherical brush can be in the collapsed state, form a star-like structure with each arm of the star being a cylindrical bundle consisting of many polyelectrolyte chains, and adopt a micelle-like structure with almost a neutral core and a charged corona (see Figure 1). These different brush conformations appear as a result of the optimization of the electrostatic interactions between charges and short-range monomer−monomer interactions. The relative importance of different factors controlling brush conformation is manifested in a nonmonotonic dependence of the brush thickness on the value of the Bjerrum length, which controls the strength of the electrostatic interactions. At small values of the Bjerrum length, the strong short-range monomer−monomer attraction causes the polyelectrolyte brush to collapse, forming a dense polymeric layer surrounding the central nanoparticles. Increasing the value of the Bjerrum length leads to the instability of the collapsed polymeric layer and formation of a star of bundles. This star of bundles conformation minimizes the electrostatic interactions between charges and the surface energy contribution streaming from the short-range Lennard−Jones interactions between monomers. With an increasing value of the Bjerrum length, the aggregation number of each arm of the star of bundles decreases while the number of bundles increases. At the value of the Bjerrum length $l_B > 0.1\sigma$, the condensed counterions start to play an important role in determining the brush conformations. At the intermediate values of the Bjerrum length $0.1\sigma < l_B < 2\sigma$, the condensed counterions reduce the effective charge of the brush by filling the brush interior. This is manifested in the reduced rate of the increase in the brush thickness with the increase of the value of the Bjerrum length (see Figure 2). However, for the values of the Bjerrum length $l_B > 3\sigma$, the correlation-induced attraction between the condensed counterions and charged monomers determines the brush structure. In this interval of the Bjerrum length, the condensed counterions facilitate the collapse of the central part of the brush, forcing a spherical brush to adopt a micelle-like structure with a dense, almost neutral core and charged corona (see Figure 8). The core of the micelle is comprised of the condensed counterions and sections of the polyelectrolyte chains, while the excess charge is expelled to the micellar corona. For very large values of the Bjerrum length $l_B > 9\sigma$, a polyelectrolyte brush forms a dense layer covering the central nanoparticles consisting of both counterions and polymers.

In our simulations, we did not observe a necklace-like structure of polyelectrolytes[38−44] forming a brush in poor solvent conditions for the polymer backbone. This is due to the fact that for our grafting densities and chain degree of polymerization the lowest energy state corresponds to the bundles of polyelectrolyte chains. However, we expect formation of the necklaces for lower values of the grafting densities and larger chain degrees of polymerization. The search for the stability region of the necklace structure in a polyelectrolyte brush in poor solvent conditions for the polymer backbone will be a subject of future study.

It is interesting to point out that similar conformational transformations in the polyelectrolyte brush can also be triggered by changing the counterion valence, introducing divalent, trivalent, or multivalent counterions. By changing the counterion valence, the energy of the electrostatic attraction between the condensed counterions and charged monomers can be increased.[48] It was observed that the polyelectrolyte brush collapses in the presence of the multivalent ions.[50,51] Thus, it is possible that multivalent ions could induce the formation of a star of bundles in the case of the spherical polyelectrolyte brush and a forest of bundles in the case of the planar brush. We hope that this paper will inspire experimentalists to search for such structures.

Acknowledgment. The authors are grateful for support of this research to the Donors of the American Chemical Society Petroleum Research Fund under Grant PRF#44861-AC7 and the National Science Foundation under Grant DMR-0353894.

Appendix A: Scaling Model of the Spherical Polyelectrolyte Brush in Poor Solvent

In this section, we present the scaling model of the bundle formation for the charged spherical brush. Our scaling model extends the approach developed in ref 27 to the case of spherical brush and cylindrical bundle formation. We begin our discussion with the case when the chain collapse is driven by the short-range monomer−monomer interactions. Consider a spherical brush of polyelectrolyte chains with a degree of polymerization N attached to the spherical particle with a radius R. There are N_{ch} polyelectrolyte chains attached to the spherical particle, which corresponds to the area per chain s_0 to be on the order of R^2/N_{ch}. Each polyelectrolyte chain is partially charged with the fraction of charged monomers f. The fraction x of counterions is condensed inside the spherical brushes, reducing the effective charge of each polyelectrolyte chain to $e(1 - x)fN = e\Delta fN$.

Stability Condition of the Collapsed Charged Brush. In poor solvent conditions for the polymer backbone, the neutral polymer brush is collapsed, forming a dense polymeric layer covering the particle surface. The equilibrium monomer density inside the dense layer is determined by balancing the second and third virial terms in the virial expansion of the monomer−monomer interaction part of the brush free energy in the power series of the monomer density ρ[52,53]

$$\frac{F^{sh}_{brush}}{k_BT} \approx N_{ch}Nb^3\tau\rho + N_{ch}Nb^6\rho^2 \qquad \text{(A1)}$$

where $\tau = 1 - \theta/T$ is the effective temperature, θ is the theta temperature, and b is the bond length. The effective temperature τ is negative in poor solvent conditions. The equilibrium monomer density inside a collapsed layer is equal to $\rho b^3 \approx |\tau|$. Note that the calculations of the equilibrium polymer density inside a collapsed brush are only correct if the absolute value of the effective temperature is smaller than unity, $|\tau| < 1$. The dense polymeric layer can be envisioned as a dense packing of thermal (correlation) blobs with size ξ and as having g monomers each filling the volume of the brush. The statistics of the chain inside the thermal blob are unperturbed by the short-range monomer−monomer attraction such that the number of monomers inside a thermal blob is related to the blob size as $\xi \approx b\sqrt{g}$. The dense packing condition of the thermal blobs leads to the following relations between the blob size, the number of monomers per blob, and the effective temperature

$$\xi \approx b/|\tau| \qquad \text{and} \qquad g \approx |\tau|^{-2} \qquad \text{(A2)}$$

(50) Tran, Y.; Auroy, P.; Lee, L. T.; Stamm, M. *Phys. Rev. E* **1999**, *60*, 6984−6990.
(51) Mei, Y. et al. *Phys. Rev. Lett.* **2006**, *97*, 158301-1−158301-4.
(52) Grosberg, A. Y.; Khokhlov, A. R. *Statistical Physics of Macromolecules*; AIP Press: College Park, MD, 1994.
(53) Rubinstein, M.; Colby, R. H. *Polymer Physics*; Oxford University Press: New York, 2003.

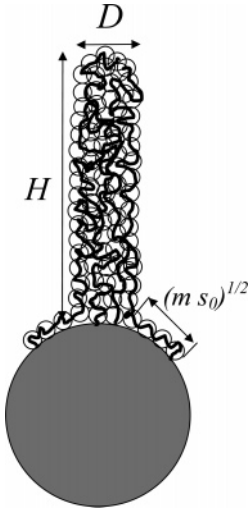

Figure 12. Schematic sketch of the blob structure of the bundle of polyelectrolyte chains.

The contribution of the monomer−monomer interactions to the brush free energy is on the order of the thermal energy k_BT per thermal blob

$$\frac{F^{sh}_{brush}}{k_BT} \approx -\frac{N_{ch}N}{g} \approx -N_{ch}N\tau^2 \quad \text{(A3)}$$

The brush thickness is determined by the packing condition, $NN_{ch}/H^3 \approx \rho$, resulting in

$$H_{CB} \approx \frac{(NN_{ch})^{1/3}}{\rho^{1/3}} \approx b(NN_{ch}/|\tau|)^{1/3} \quad \text{(A4)}$$

Here and below, we will assume that the brush thickness H is larger than the size of the central particle R. In addition to the bulk contribution, the collapsed brush has a surface energy contribution, which is due to the polymer−solvent interface.

$$F_{surf} \approx \gamma H^2 \quad \text{(A5)}$$

where γ is the surface energy of the polymer−solvent interface. The origin of the surface energy is the difference in the number of the nearest neighbors for the thermal blobs at the surface of the brush and for the thermal blobs inside the collapsed brush. The energy associated with the polymer−solvent interface can be estimated as the thermal energy k_BT per thermal blob on the brush surface, $\gamma \approx k_BT/\xi^2$.[52,53]

If the brush is charged, there is an electrostatic repulsion between uncompensated charges within the collapsed brush layer. The energy of the electrostatic repulsion is equal to

$$\frac{U_{elect}}{k_BT} \approx \frac{l_B(\Delta fNN_{ch})^2}{H_{CB}} \quad \text{(A6)}$$

where we have introduced $\Delta f = (1 - x)f$, as the effective fraction of charged monomers, for small fractions of the condensed counterions, $x \ll 1$; this parameter is on the order of the fraction of the charged monomers f, $\Delta f \approx f$. The strength of the electrostatic interactions is controlled by the value of the parameter $l_B\Delta f^2$. This parameter varies with the value of the Bjerrum length or fraction of the ionized groups, f. The collapsed brush will maintain its spherical shape as long as the brush surface energy is larger than the electrostatic repulsion between charges within a collapsed brush. The stability condition is obtained by equating the brush surface energy (eq A5) with its electrostatic energy. This results in

$$(u\Delta f^2)_{CB} \approx \frac{|\tau|}{N_{ch}N} \quad \text{(A7)}$$

where u is the ratio of the Bjerrum length l_B to the bond size b, $u = l_B/b$. Note that the stability condition of eq A7 is similar to the stability condition of the charged spherical globule formed by the polyelectrolyte chain in poor solvent conditions for the polymer backbone. If the interaction parameter $u\Delta f^2$ is larger than the critical value, the spherical brush becomes unstable and transforms into a star, each arm of which is a bundle of polyelectrolyte chains (star of bundles). This brush configuration minimizes the energy of the electrostatic repulsion in comparison with that of the spherical brush. Interestingly, the transformation of the shape of the spherical brush occurs at a constant brush volume, which is controlled by the short-range interactions.

Bundle Formation Due to Two-Body Monomer−Monomer Attraction. Let us assume that each bundle consists of m polyelectrolyte chains with height H and radius D (see Figure 12). The surface energy of a cylindrical bundle is equal to

$$F_{surf} \approx \frac{k_BT}{\xi^2}(DH + D^2) \quad \text{(A8)}$$

The grafting points of the m-polyelectrolyte chains assembled into the bundle are distributed over the surface area ms_0 where s_0 is the surface area per grafted chain, $s_0 \approx R^2/N_{ch}$. Thus, each polyelectrolyte chain should extend an average distance on the order of $(ms_0)^{1/2}$ before reaching the bundle.[27] This will impose an additional energetic penalty on the order of the thermal energy k_BT per each thermal blob in the string of monomers of length $(ms_0)^{1/2}$. This contribution to the bundle free energy is equal to

$$F_{str} \approx k_BTm^{3/2}s_0^{1/2}/\xi \quad \text{(A9)}$$

The electrostatic energy of the star of bundles includes the energy of the electrostatic repulsion between charges within the same bundle and the interbundle electrostatic repulsion. When the number of bundles is relatively small, $N_{ch}/m < 10$, the intrabundle electrostatic energy dominates over its interbundle counterpart. In this case, the electrostatic energy is approximated as

$$U_{elect} \approx k_BT\frac{l_B(\Delta fNm)^2}{H} \quad \text{(A10)}$$

Note that in eq A10 we have neglected the logarithmic correction to the bundle electrostatic energy.

Combining all terms together (eqs A8−A10) and multiplying the single bundle free energy contributions by the number of bundles N_{ch}/m, we finally arrive at the following expression for the total free energy of the spherical brush of bundles

$$\frac{F}{k_BTN_{ch}} \approx \frac{l_B(\Delta fN)^2m}{H} + \frac{HD}{m\xi^2} + \frac{D^2}{m\xi^2} + \frac{(ms_0)^{1/2}}{\xi} - N/g \quad \text{(A11)}$$

To find the equilibrium parameters of the bundle, eq A11 has to be minimized with respect to the height of the bundle H and its aggregation number m at the additional constraint

$$\rho D^2 H \approx mN \tag{A12}$$

which fixes the total volume of the bundle to a value controlled by the short-range monomer−monomer interactions. This equation provides a relation between the width of the bundle D, its height, and the aggregation number m, $D \approx (mN/\rho H)^{1/2}$. The height of the bundle H is obtained by minimizing the first and second terms in the right-hand side (rhs) of eq A11 with respect to H. This leads to

$$H_{\mathrm{I}} \approx b(u\Delta f^2)^{2/3} mN/|\tau| \tag{A13}$$

Thus, the equilibrium bundle length is a result of the optimization of the bundle electrostatic energy, which tends to increase both the brush size and the bundle surface energy that opposes such an increase to minimize the surface area of the polymer−solvent interface. Substitution of eq A13 for the bundle height into eq A12 shows that the bundle width D is independent of the bundle height H and the bundle aggregation number m

$$D_{\mathrm{I}} \approx b(u\Delta f^2)^{-1/3} \tag{A14}$$

The fact that the bundle width is on the order of the electrostatic blob (bead) size in poor solvent conditions for the polymer backbone is noteworthy.

The equilibrium aggregation number of the bundle, m, is obtained by balancing the surface energy of the top of the cylinder (the third term in the rhs of eq A11) and the free energy of the strings (the fourth term in the rhs of eq A11), which results in

$$m_{\mathrm{I}} \approx \frac{|\tau|^{2/3}}{(u\Delta f^2)^{4/9}} \left(\frac{b^2}{s_0}\right)^{1/3} \tag{A15}$$

The length of the bundle with the aggregation number m is equal to

$$H_{\mathrm{I}} \approx b \frac{(u\Delta f^2)^{2/9}}{|\tau|^{1/3}} \left(\frac{b^2}{s_0}\right)^{1/3} N \tag{A16}$$

As one can see, eqs A14−A16 do not have dependence on the number of chains N_{ch} forming the spherical brush. This is due to the fact that the parameters of the bundle are only determined by the intrabundle free energy contributions.

The electrostatic repulsion between the arms of the star of the bundles becomes important when $N_{\mathrm{ch}}/m_{\mathrm{I}} > 10$. The crossover to this regime occurs at

$$(u\Delta f^2)_{\mathrm{II}} \approx \frac{|\tau|^{3/2}}{N_{\mathrm{ch}}{}^{9/4}} \left(\frac{b^2}{s_0}\right)^{3/4} \approx \left(\frac{|\tau| b}{N_{\mathrm{ch}} R}\right)^{3/2} \tag{A17}$$

Thus, the electrostatic repulsion between the arms of the star controls the brush size for the range of the interaction parameter $u\Delta f^2$ larger than $(u\Delta f^2)_{\mathrm{II}}$.

In this regime, the energy of the electrostatic interactions of the spherical brush is equal to

$$U_{\mathrm{elect}} \approx k_{\mathrm{B}}T \frac{l_{\mathrm{B}}(\Delta f N N_{\mathrm{ch}})^2}{H} \tag{A18}$$

With this electrostatic energy, the free energy per chain of the spherical brush in the star of bundles configuration is written as follows:

$$\frac{F}{k_{\mathrm{B}}TN_{\mathrm{ch}}} \approx \frac{l_{\mathrm{B}}(\Delta f N)^2 N_{\mathrm{ch}}}{H} + \frac{HD}{m\xi^2} + \frac{D^2}{m\xi^2} + \frac{(ms_0)^{1/2}}{\xi} - N/g \tag{A19}$$

Repeating the same minimization procedure as before, we obtain the following expressions for the bundle height

$$H_{\mathrm{II}} \approx b|\tau|^{-3/5}(u\Delta f^2)^{2/5} N N_{\mathrm{ch}}{}^{2/5} \left(\frac{b^2}{s_0}\right)^{1/5} \tag{A20}$$

width

$$D_{\mathrm{II}} \approx b(u\Delta f^2)^{-3/5} \left(\frac{|\tau| b}{N_{\mathrm{ch}} R}\right)^{2/5} \tag{A21}$$

and bundle aggregation number

$$m_{\mathrm{II}} \approx \frac{|\tau|^{6/5}}{(u\Delta f^2)^{4/5} N_{\mathrm{ch}}{}^{4/5}} \left(\frac{b^2}{s_0}\right)^{3/5} \tag{A22}$$

With an increasing value of the parameter u, the fraction of condensed counterions inside the brush increases as well. This increase of the fraction of the condensed counterions leads to a decrease in the energy of the electrostatic repulsion between uncompensated charges within the spherical brush. At the same time, the counterion entropy contribution to the spherical brush free energy increases, since more counterions are localized within the brush volume. Finally, when the counterion entropy becomes larger than the electrostatic energy of the brush, the crossover to the so-called "osmotic brush" regime takes place. In this regime, the configurational entropy of counterions determines the brush swelling. The osmotic contribution to the brush free energy due to localization of the $xfNN_{\mathrm{ch}}$ counterions is

$$F_{\mathrm{osm}} \approx k_{\mathrm{B}}TxfNN_{\mathrm{ch}} \ln(xfNN_{\mathrm{ch}} b^3/H^3) \tag{A23}$$

In writing the equation above, we have assumed that counterions are uniformly distributed over the brush volume. If most of the counterions are localized within the bundles, we have to change H^3 in eq A23 to $N_{\mathrm{ch}}HD^2/m$ to account for the total volume occupied by the bundles. It is important to point out that on the scaling level such substitution does not lead to any new scaling law describing the parameters of the bundle, such as bundle length H, width D, and bundle aggregation number m. In the osmotic regime, the free energy per chain is written as

$$\frac{F}{k_{\mathrm{B}}TN_{\mathrm{ch}}} \approx xfN \ln\left(\frac{xfNN_{\mathrm{ch}} b^3}{H^3}\right) + \frac{HD}{m\xi^2} + \frac{D^2}{m\xi^2} + \frac{(ms_0)^{1/2}}{\xi} - N/g \tag{A24}$$

Minimizing eq A24 with respect to H and m, we find that the equilibrium width D of the bundle is

$$D_{\mathrm{osm}} \approx b|\tau|/(xf) \tag{A25}$$

Each bundle consists of

$$m_{osm} \approx \frac{\tau^2}{(xf)^{4/3}}\left(\frac{b^2}{s_0}\right)^{1/3} \quad \text{(A26)}$$

polyelectrolyte chains and has a thickness of

$$H_{osm} \approx b\frac{(xf)^{2/3}}{|\tau|}\left(\frac{b^2}{s_0}\right)^{1/3} N \quad \text{(A27)}$$

The crossover to the osmotic regime occurs at the value of the interaction parameter $u\Delta f^2$

$$(u\Delta f^2)_{osm} \approx \frac{(xf)^{5/3}}{|\tau|N_{ch}}\left(\frac{b^2}{s_0}\right)^{1/3} \quad \text{(A28)}$$

The last equation was obtained by equating the brush thicknesses H_{II} and H_{osm}.

Brush Structure in the Case of Fluctuation/Correlation-Induced Attraction. In the interval of large Bjerrum lengths or at a sufficiently large fraction, x, of the condensed counterions, the fluctuations in the counterion density inside the brush can lead to strong correlation/fluctuation-induced attractive interactions between counterions and charged monomers. This attraction can be stronger than the two-body monomer−monomer attractive interactions. Let us first consider the case of the completely collapsed brush. The correlation-induced attractive interaction energy between the counterions and the neutralizing background of the collapsed brush is equal to (for details, see refs 42 and 54)

$$\frac{U_{OCP}}{k_BT} \approx -N_{ch}Nxf\begin{cases} l_B/\xi_c, & \text{for } \xi_c \le l_B \\ (l_B/\xi_c)^{3/2}, & \text{for } \xi_c \gg l_B \end{cases} \quad \text{(A29)}$$

where $\xi_c \approx (xf\rho)^{-1/3}$ is the typical distance between condensed counterions inside the bundle with an average monomer density ρ. The two different regimes in eq A29 correspond to strongly, $\xi_c < l_B$, and weakly, $\xi_c > l_B$, correlated condensed counterions.

In this regime, the equilibrium polymer density inside a bundle is obtained by minimizing the three-body interaction term in eq A1 with the correlation-induced attractive interaction energy given by eq A29 with respect to the polymer density ρ. This results in the following expression for the polymer density inside a collapsed brush:

$$\rho b^3 \approx \begin{cases} u^{3/5}(xf)^{4/5}, & \text{strongly correlated} \\ uxf, & \text{weakly correlated} \end{cases} \quad \text{(A30)}$$

Once again, the correlation blob picture can be used to describe the polymer density fluctuations inside a collapsed brush with polymer density ρ. This results in the number of monomers in a correlation blob to be

$$g \approx \begin{cases} u^{-6/5}(xf)^{-8/5}, & \text{strongly correlated} \\ (uxf)^{-2}, & \text{weakly correlated} \end{cases} \quad \text{(A31)}$$

and the correlation blob size to be equal to

$$\xi \approx b\begin{cases} u^{-3/5}(xf)^{-4/5}, & \text{strongly correlated} \\ (uxf)^{-1}, & \text{weakly correlated} \end{cases} \quad \text{(A32)}$$

In the case when condensed counterions drive brush collapse, the origin of the surface energy is the difference in the number of the nearest neighbors for the condensed counterions at the surface of the brush and the counterions inside the brush. In the case of the strongly correlated counterion system, the surface energy of a brush is estimated to be the product of the number of condensed counterions at the brush surface H^2/ξ_c^2 and the energy of the electrostatic interaction between a counterion and its neutralizing background k_BTl_B/ξ_c

$$F_{surf} \approx k_BT\frac{l_B}{\xi_c^3}H^2 \quad \text{(A33a)}$$

The surface energy of a brush in the weakly correlated case is k_BT per correlation blob of size ξ at the surface of the brush. Taking this into account, the surface energy term is

$$F_{surf} \approx \frac{k_BT}{\xi^2}H^2 \quad \text{(A33b)}$$

The height of the brush layer collapsed by the condensed counterions is equal to

$$H_{CB} \approx \frac{(NN_{ch})^{1/3}}{\rho^{1/3}} \approx b(NN_{ch})^{1/3}\begin{cases} u^{-1/5}(xf)^{-4/15}, & \text{strongly correlated} \\ (uxf)^{-1/3}, & \text{weakly correlated} \end{cases} \quad \text{(A34)}$$

In this regime, the thickness of the brush decreases when both the value of the parameter u and the fraction of the condensed counterions x increase.

Now let us discuss the transformation of the collapse brush as the fraction of the condensed counterions decreases. In the case when the brush collapse is caused by condensed counterions, the polyelectrolyte brush can maintain an almost neutral core by expelling the chain sections (fingers) with extra charge. Thus, there will be fingering instability of the brush interface, and the brush can have the structure of a star-like micelle with a collapsed, almost neutral core and charged corona (see Figure 13). The excess charge, which each expelled chain from the dense core section of the polyelectrolyte chain with N_{out} monomers can carry, is equal to efN_{out}. If the net charge of the brush is equal to $e\Delta fN_{ch}N$, one will need m_{out} chain sections to carry these extra

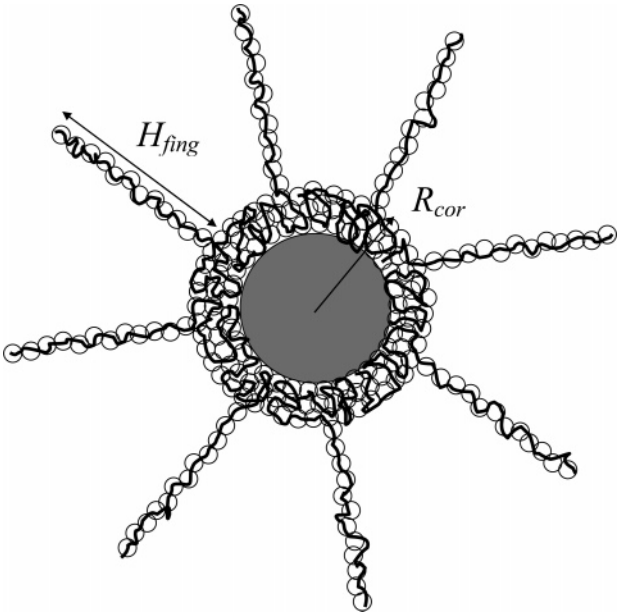

Figure 13. Schematic sketch of the blob structure of the micelle-like brush structure.

(54) Brilliantov, N. V.; Kuznetsov, D. V.; Klein, R. *Phys. Rev. Lett.* **1998**, *81*, 1433−1436.

charges into the corona.

$$f m_{out} N_{out} \approx \Delta f N_{ch} N \tag{A35}$$

This process of partial chain expulsion is favorable if the electrostatic energy of the collapsed charged brush without expelled chains is larger than the loss of the attraction energy which each expelled chain has lost by leaving the collapsed core. This energy loss can be estimated as the thermal energy k_BT per each correlation blob, $\Delta U \approx k_B T N_{out}/g$, where g is given by eq A31. Comparing these energies, one finds that

$$\frac{l_B(\Delta f N_{ch} N)^2}{H_{CB}} \approx \frac{m_{out} N_{out}}{g} \approx \frac{\Delta f N_{ch} N}{fg} \tag{A36}$$

or solving for the fraction of uncompensated charge Δf one can derive the following expression determining the transition to the star-like micelle conformation in the case of strong correlations

$$\Delta f_{FI} \approx f^{1/3} x^{4/3} (N_{ch} N)^{-2/3} \tag{A37}$$

The equilibrium parameters of the star-like micelle with m_{out} chains forming a corona of the micelle, each of which having N_{out} monomers, are obtained by minimizing the corona free energy that includes the energy of the electrostatic repulsion between excess charges within a brush, the elastic energy of the stretched chains in the corona, and the increase of the micelle free energy due to displacement of monomers into the corona

$$\frac{F_{corona}}{k_B T} \approx \frac{l_B(\Delta f N_{ch} N)^2}{R_{cor} + H_{fing}} + m_{out} \frac{H_{fing}^2}{b^2 N_{out}} + m_{out} N_{out}/g \tag{A38}$$

The size of the core is controlled by the correlation-induced attractive interactions and is given by eq A34, in which one has to substitute the total brush mass, $N_{ch}N$, for the mass of the monomers remaining in the core $N_{ch}N - m_{out}N_{out}$. To find the equilibrium parameters of the corona, the free energy of the corona, eq A38, has to be minimized with respect to N_{out}, m_{out}, and H_{fing} at the additional constraint that all excess charge is moved into the corona (eq A35). Minimization of the last two terms in eq A38 with respect to the number of expelled monomers N_{out} results in

$$H_{fing} \approx b N_{out}/g^{1/2} \approx \xi N_{out}/g \tag{A39}$$

Thus, the sections of the chains in the corona of the micelle are strongly stretched and can be viewed as arrays of correlation blobs. Substitution of eq A39 into eq A38 eliminates the dependence on the number of monomers N_{out}

$$\frac{F_{corona}}{k_B T} \approx \frac{l_B(\Delta f N_{ch} N)^2}{R_{cor} + H_{fing}} + m_{out} \frac{H_{fing}}{\xi} \tag{A40}$$

The equilibrium thickness of the corona is obtained by minimizing the remaining terms with respect to H_{fing}

$$m_{out} \approx \frac{\xi l_B(\Delta f N_{ch} N)^2}{(R_{cor} + H_{fing})^2} \approx \frac{\xi l_B(\Delta f N_{ch} N)^2}{H_{fing}^2} \tag{A41}$$

In transforming eq A41, we have assumed that the thickness of the corona is larger than the size of the core. The last equation can be solved for the corona thickness by taking into account eqs A35 and A39

$$H_{fing} \approx l_B f g \Delta f N_{ch} N \approx b \Delta f N_{ch} N \begin{cases} u^{-1/5} f^{-3/5} x^{-8/5}, & \text{strongly correlated} \\ u^{-1} f^{-1} x^{-2}, & \text{weakly correlated} \end{cases} \tag{A42}$$

It follows from this equation that the thickness of the brush should decrease as the number of the condensed counterions inside it increases.

The number of monomers in each expelled chain is given by the following equation:

$$N_{out} \approx u f g^{3/2} \Delta f N_{ch} N \approx \Delta f N_{ch} N \begin{cases} u^{-4/5} f^{-7/5} x^{-12/5}, & \text{strongly correlated} \\ u^{-2} f^{-2} x^{-3}, & \text{weakly correlated} \end{cases} \tag{A43}$$

Since part of the expelled chain resides inside the core, the number of expelled monomers cannot exceed

$$N_{out} \le N - R_{cor}^2/b^2 \approx N \tag{A44}$$

Thus, when the number of monomers N_{out} becomes of the order of N, which happens by

$$\Delta f \approx N_{ch}^{-1} \begin{cases} u^{4/5} f^{7/5} x^{12/5}, & \text{strongly correlated} \\ u^2 f^2 x^3, & \text{weakly correlated} \end{cases} \tag{A45}$$

the mass of the corona growing by expelling more and more chains

$$m_{out} \approx \Delta f N_{ch}/f \tag{A46}$$

In the case of the brush collapse caused by correlation-induced attraction, the transition between this micelle-like structure of the brush and a brush of bundles occurs when the number of monomers in the correlation blob g becomes on the order of the number of monomers in the correlation blob in which the short-range interactions are responsible for the brush collapse. Combining eqs A2 and A31, one obtains

$$|\tau| \approx \begin{cases} u^{3/5} (xf)^{4/5}, & \text{strongly correlated} \\ uxf, & \text{weakly correlated} \end{cases} \tag{A47}$$

These two equations determine the line of the first-order transition.

It is interesting to point out that the bundle formation can also be described in the framework of the microphase separation model developed by Olvera de la Cruz et al.[55,56] In this case, the bundle formation is a result of the optimization of the electrostatic and surface energies of the counterion and polymer rich domains. The comparison between our model and the microphase separation model will be the subject of a future publication.

LA702203C

(55) Solis, F. J.; Stupp, S. I.; Olvera de la Cruz, M. *J. Chem. Phys.* **2005**, *122*, 054905-1−9.
(56) Loverde, S. M.; Solis, F. J.; Olvera de la Cruz, M. *Phys. Rev. Lett.* **2007**, *98*, 237802-1−4.